Evaluation of portable X-ray fluorescence for exploration of carbonate-hosted sulfide mineralisation, Otavi Mountain Land, Namibia

E. Shalimba[1]*, S. Lohmeier[2], A. Wanke[1,3]

[1] University of Namibia, Faculty of Agriculture, Engineering & Natural Sciences, Department of Geosciences, Southern Campus, Private Bag 13302, Windhoek, Namibia

[2] Clausthal University of Technology, Mineral Resources/ Mining Engineering, Adolph-Roemer Str. 2A, 38678 Clausthal-Zellerfeld, Germany

[3]Upstream Exploration Services Namibia

* eshalimba@unam.na

Abstract

The Otavi Mountain Land province forms part of the Damara Orogenic Belt within the Neoproterozoic carbonate platform, which is well-known for its sedimentary-hosted, polymetallic mineralized horizons, including the Cu-Pb(-Ag) Kombat deposit. The mineralisation at Kombat is of massive, disseminated, veinlet-controlled and brecciated mineralisation styles. It is mainly composed of bornite, chalcopyrite, galena, covellite and chalcocite, associated with quartz and calcite as gangue minerals. Mineralized zones are distinctly enriched in chalcophile elements, including Pb, Cu, As and Ag. For the analysis of such rocks, laboratory-based analytical methods, including inductively coupled plasma mass spectrometry (ICP-MS) and atomic absorption spectroscopy (AAS), are well established, in contrast to on-site geochemical analytical methods. This study shows the applicability and limitations of portable X-ray fluorescence (pXRF) in the geochemical exploration of sulfide (Ag, Cu, Fe, Mn, Pb, Zn) ores in carbonate matrix. Additional ICP-MS/AAS data and certified reference materials are used to assess the applicability of such portable tools for Kombat-type ores. This study shows that elements like Cu, Fe, Mn, Pb and Zn (RSD $\leq$10%) can be analysed with excellent or very good precision by pXRF, while other elements (Ag, Sr) show poor precision. The trace element concentrations obtained by pXRF are comparable to ICP-MS results yielding a good correlation ($R^2 \geq 0.85$) and acceptable accuracy and precision. Portable XRF is identified as a low-cost tool that can be used successfully in the geochemical exploration for a list of elements in carbonate-hosted sulfide ores.

Keywords: Portable XRF, sulfide mineralisation, carbonate host rock, Otavi Mountain Land, Namibia

Received: December 2024
Received in revised form: April 22, 2025
Accepted: June 27, 2025
Published: July 2, 2025

1. Introduction

To date, one of the greatest challenges in exploration and mining are operational costs as the costs of sampling and sample analyses can be considerably high. Over the past years, portable X-ray fluorescence (pXRF) has been extensively and successfully used in the exploration of base metals, rare earth elements (REEs) and precious metals linked to magmatic and sedimentary rocks (Simandl et al., 2014a; Gazley and Fisher, 2014; Hall et al., 2014; Quye-Sawyer et al., 2015). However, there is a distinct lack in knowledge of the applicability of this tool for low-grade, carbonate-hosted sulfidic ores. So far, application of pXRF in geochemical exploration is recognised as a viable method which can be employed to obtain a reliable dataset during field mapping, and which assists in sample selection (Young et al., 2016). This instrument has two advantages: a) it allows direct, on-site measurements of selected elements and thus offers a dataset, that provides valuable insights in mining and exploration, leading to rapid field decisions and, b) it is cost-effective (Andrew and Barker, 2017; Lemière, 2018). However, in order to optimise results obtained by pXRF, there is a need to (re-)calibrate the instrument using certified reference materials (CRMs) with the same matrix as the samples of interest (Simandl et al., 2014b; Gallhofer and Lottermoser, 2018), as it is common practice for conventional laboratory based XRF devices. Portable XRF results, when compared to known samples, such as CRMs, yield a moderate to high precision but there is usually a high variation when it comes to accuracy (Piercey and Devine, 2014). Hall et al. (2014) showed that pXRF performance is different for various elements. Elements such as Cu and Pb are recorded with a very good performance, whereas performance is moderate for Cr and U, but poor for Ag and V, and extremely poor for elements like W and Au. Limitations and capabilities of a pXRF device, as well as a quality control of the dataset obtained by pXRF are discussed in detail in Arne and Jeffress (2014), Brand and Brand (2014), Fisher et al. (2014), and Hall et al. (2014). This study aims to investigate whether the low-cost technique pXRF can be applied in the exploration of carbonate-hosted sulfide base metal deposits of the Otavi Mountain Land (OML). Neoproterozoic carbonate rocks are known to host a variety of base metal deposits that are important for the world supply of metals such as Pb and Zn (Leach et al., 2010; Haest and Muchez, 2011; Xiong et al., 2019). The Otavi Mountain Land (OML) is a metallogenic province in Namibia, well known for its sediment-hosted ore deposits rich in base metal sulfides and oxides, with the most economic ones concentrated in the upper part of the Neoproterozoic carbonate platform of the Damara Orogenic Belt (DOB) (Figs 1, 2) (Miller, 1983; Melcher et al., 2006; Boni et al., 2007; Kamona and Günzel, 2007). Most of the base metal deposits, including Tsumeb, Kombat, Berg Aukas, Abenab West and Khusib Spring are hosted in the sedimentary units of the Otavi Group (Melcher et al., 2006; Kamona and Günzel, 2007; Fig. 1). The Kombat deposit is a stratabound, syntectonic Cu-Pb(-Ag) sulfide deposit hosted in the dolomite of the Hüttenberg Formation (Deane, 1995). The mineralisation is mainly related to the contact between Hüttenberg dolomite and phyllite, and its genesis is associated with a magmatic hydrothermal event (Kamona and Günzel, 2007). Exploration and mining in the OML dates back to the 1920s and is still ongoing.

Therefore, mineralogical, petrological and bulk rock trace element geochemical analyses of the carbonate-hosted Cu-Pb-Zn sulfide mineralisation – with 18.5 Mt of ore mined at a grade of 2.15 wt.% Pb, 2.79 wt.% Cu, 1.5 wt.% Zn, and 125 g/t Ag (Kamona and Günzel, 2007) – of the Kombat deposit are integrated. The applicability and the limitations of the pXRF device for analysis of such rocks are investigated by comparing results from pXRF with those from inductively coupled plasma mass spectrometry (ICP-MS) and atomic absorption spectroscopy (AAS). Precision and accuracy of the pXRF instrument is assessed using pXRF results of CRMs.

2. Geological setting

The Neoproterozoic Damara Orogen forms part of the west Gondwana suture, which resulted from the collision of the South American Río de la Plata with the Southern African Congo, and Kalahari cratons (Miller, 1983; Gray et al., 2008). In Namibia, this orogen is sub-divided into three-fold belts: the NNW-trending northern coastal Kaoko Belt, the ENE-trending inland branch DOB and the S-trending southern coastal Gariep Belt (Martin and Porada, 1977; Miller, 1983, 2008). The DOB is a ~350 km wide belt (Fig. 3), which formed during continuous stages of crustal thickening, rifting, spreading, and subduction followed by continental collision, upper lithospheric thinning, and finally continental collision between the Kalahari and Congo Cratons, ending with the closure of the Khomas Sea (Porada, 1979; Miller, 1983; Gray et al., 2008; Goscombe et al., 2018). The DOB consists of basement inliers of Archean-Proterozoic age, early Damaran rift type sedimentary and volcanic units of the Nosib Group, Neoproterozoic deep and shallow carbonate rocks of the Otavi and Swakop Groups, and foreland basin deposits of the Mulden and Nama Groups (Miller, 1983; Gray et al., 2008; Miller, 2008). Additionally, the belt is further subdivided into various tectonostratigraphic zones such as the Northern Zone and the Northern Platform (Fig. 3) that are defined by age, structure and metamorphic grade (Miller, 2008).

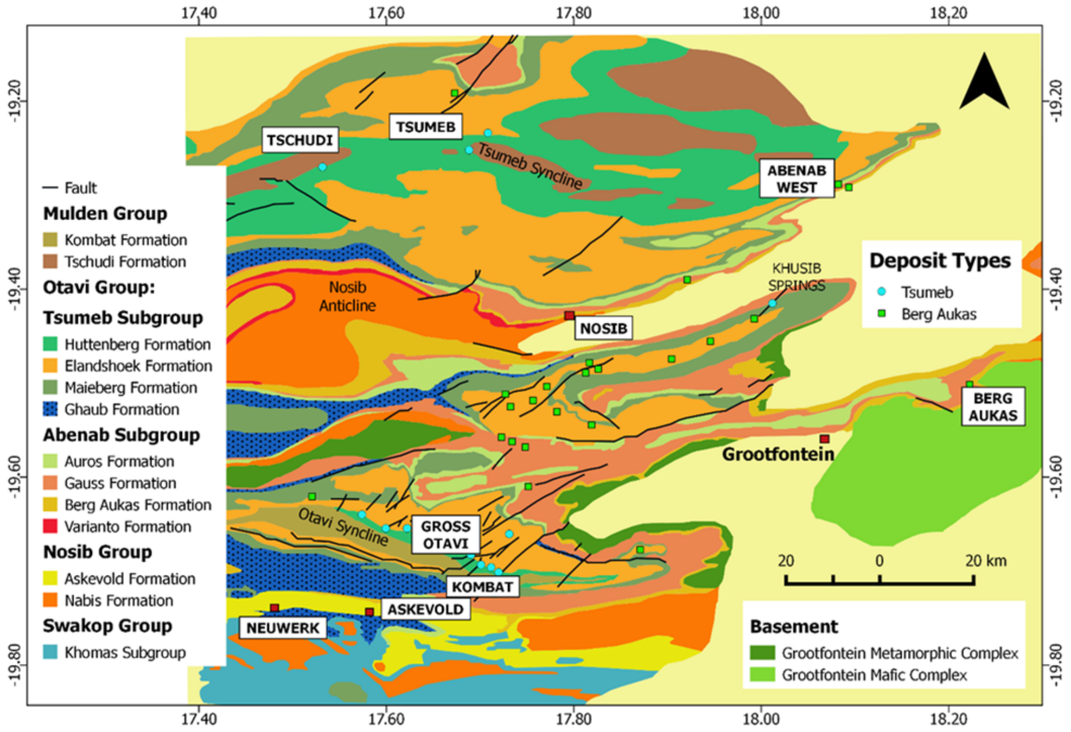

Fig. 1. Simplified regional geological map of the OML, with the outlined most important base metal deposits (modified after Chetty and Frimmel, 2000; Kamona and Günzel, 2007).

Following the initial rifting, the sediments of the Nosib Group were deposited whereas the Otavi Group was deposited during the subsequent opening of the Khomas Sea (Miller, 2008). In the Northern and Northern Platform tectonostratigraphic zones, the Otavi Group is dominated by shallow water platform successions of carbonate units that largely rest on the southern Congo Craton (Chetty and Frimmel, 2000; Hoffman, 2011). The Otavi Group carbonates are the dominant units of the base-metal rich OML province, which covers ~10,000 km^2 and is situated at the transition between the Northern Zone and the Northern Platform (Fig. 1) (Pirajno and Joubert, 1993; Kamona and Günzel, 2007). This province is associated with three Damara deformation episodes: D1-D3. During the first tectonic event D1, the southern part of the OML was folded and faulted (Miller, 1983). The ultimate collision of the Congo and Kalahari Cratons led to the D2 and D3 tectonic events. D3 is attributed to post-Damara deformation processes (Kröner, 1982; Miller, 1983; Goscombe et al., 2004; Schneider et al., 2008).

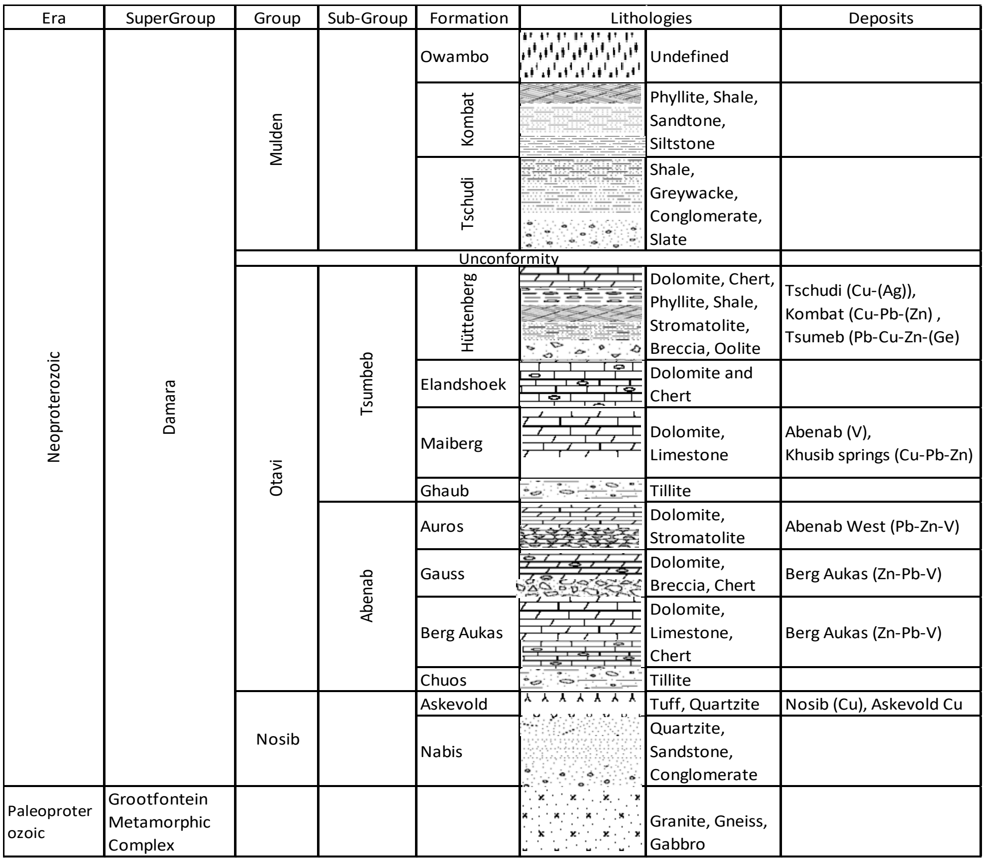

Era	SuperGroup	Group	Sub-Group	Formation	Lithologies	Deposits
Neoproterozoic	Damara	Mulden		Owambo	Undefined	
				Kombat	Phyllite, Shale, Sandtone, Siltstone	
				Tschudi	Shale, Greywacke, Conglomerate, Slate	
		Unconformity				
		Otavi	Tsumbeb	Hüttenberg	Dolomite, Chert, Phyllite, Shale, Stromatolite, Breccia, Oolite	Tschudi (Cu-(Ag)), Kombat (Cu-Pb-(Zn)) , Tsumeb (Pb-Cu-Zn-(Ge))
				Elandshoek	Dolomite and Chert	
				Maiberg	Dolomite, Limestone	Abenab (V), Khusib springs (Cu-Pb-Zn)
				Ghaub	Tillite	
			Abenab	Auros	Dolomite, Stromatolite	Abenab West (Pb-Zn-V)
				Gauss	Dolomite, Breccia, Chert	Berg Aukas (Zn-Pb-V)
				Berg Aukas	Dolomite, Limestone, Chert	Berg Aukas (Zn-Pb-V)
				Chuos	Tillite	
		Nosib		Askevold	Tuff, Quartzite	Nosib (Cu), Askevold Cu
				Nabis	Quartzite, Sandstone, Conglomerate	
Paleoproterozoic	Grootfontein Metamorphic Complex				Granite, Gneiss, Gabbro	

Fig. 2. Stratigraphic column of the OML showing the main base-metal ore deposits in that region (modified after Kamona and Günzel, 2007).

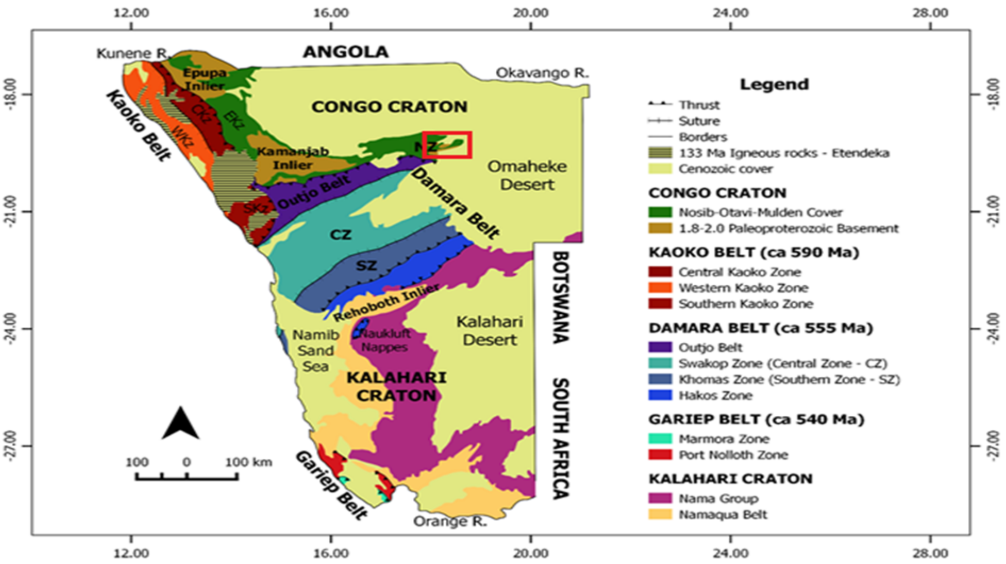

Fig. 3. Simplified geological map of Namibia, showing the various tectonostratigraphic units of the Damara Orogen. The study area, the OML, is shown by the red box (modified after Hoffman, 2013).

3. Local geological setting

The OML unconformably overlies the Paleoproterozoic basement rocks of the Grootfontein Metamorphic Complex which is mainly composed of dolomites and calc-silicate rocks, as well as the Grootfontein Mafic Bodies which are mainly composed of anorthosites and gabbros (Fig. 2) (Miller, 1983; Kamona and Günzel, 2007; Schneider et al., 2008). This carbonate platform in the OML is known for its various clusters of epigenetic mineralisation related to two major mineralisation types: the Tsumeb-type mineralization, which is characterised by distinct sulfide ores enriched in Ag, As, Cd, Cu, Ga, Ge, Pb and Zn, and the Berg Aukas-type mineralization, which consists of ore bodies containing Pb, Zn and V (Pirajno and Joubert, 1993; Cairncross, 1997). The most economic deposits in the OML (Tschudi, Tsumeb, Kombat, Berg Aukas, Abenab V, Tsumeb West, Askevold, Khusib Springs, Neuwerk, Nosib, Gross Otavi) contained between 157 kt and 57 Mt of ore with av. Pb contents ≤10.45 wt.% (Tsumeb), av. Cu contents ≤10.06 wt.% (Khusib Springs) and av. Zn contents ≤18.98 wt.% (Berg Aukas) as well as av. Ag of up to 584 g/t (Khusib Springs; Kamona and Günzel, 2007). The Berg Aukas-type deposits are confined to the lower Abenab Subgroup (Fig. 2). They were formed during the first mineralising event that is associated with compaction and dewatering of sediments of a northern rift (Pirajno and Joubert, 1993; Cairncross, 2021). Tsumeb-type deposits are mainly found in the Upper Tsumeb Subgroup and were formed as a result of a later metamorphic episode associated with devolatilization reactions during regional prograde metamorphism of the sediments in the northern rift (Fig. 2) (Pirajno and Joubert, 1993). Despite Pirajno and Joubert (1993) and Cairncross (2021) conclusions on the classification of the mineralisation types, controversy and debate still exists as to whether it is fully applicable on all the prospects and metal deposits in the OML.

The location of the Kombat deposit within the stratigraphy of the OML is shown in Figs 1 and 2. This deposit is located on the northern limb of the Otavi syncline and is positioned along the contact between the phyllite of the Mulden Group and the underlying dolostones of the Otavi Group (Deane, 1995; Kamona and Günzel, 2007; Minz, 2008). The uppermost part of the Otavi Group consists of dolomite, chert and breccia of the Hüttenberg Formation, while, in the Kombat area, the lowermost part of the Mulden Group consists of phyllite, slate and sandstones of the Kombat Formation (Kamona and Günzel, 2007). The deposit hosts a base metal sulfide mineralisation in fracture veins and galena-rich alteration breccias that are spatially associated with a replacement Fe-Mn oxide/silicate mineralisation (Pirajno and Joubert, 1993).

There are at least seven distinct mineralized zones identified in the Kombat deposit, which are described either as Cu-Pb-Ag Mississippi valley type (MVT) mineralization or as stratiform, syn-sedimentary Fe-Mn-type mineralization (Deane, 1995; Nghoongoloka et al., 2020). Base metal sulfide mineralisation styles include massive and semi-massive ores as well as mineralized vein fractures, which are mostly hosted in the dolomites of the Hüttenberg Formation. The primary ore minerals are chalcopyrite, bornite, galena, chalcocite, pyrite and tennantite, which are associated with sedimentary breccia, calcitized dolostone and lenses of feldspathic sandstone (Deane, 1995). Minor ore minerals include malachite and sphalerite, with calcite, dolomite, and quartz as gangue. The concentration of base metals at Kombat is attributed to the conversion of anhydrite in the dolostone to calcite via the release of SO_4 to brines by incorporation of CO_2 and CH_4 from shale of the Mulden Group (Trigon Metals, 2017). Additionally, isotope data from Deane (1995) allude to a magmatic and metamorphic source for the mineralising fluids. Structurally, genesis of this deposit is related to D2, which is coeval to the sedimentation of the Mulden Group (Deane, 1995). Alteration is widespread to locally pervasive and comprises a heterogeneous assemblage of calcite-quartz-sericite-pyrite-chalcopyrite and minor chlorite-hematite-pyrophyllite-kaolinite (Deane, 1995; Minz, 2008).

4. Materials and Methods

4.1 Sampling, sample preparation and petrography

Samples were taken from outcrops and heap dumps where rock material from underground mining activities had been stored. These samples are representative of the primary sulfide mineralization of the deposit. The samples were collected for the purpose of a geochemical, petrographic, and mineralogical study.

Sample preparation was done at the GSN laboratories. Each sample has been split into two parts, one for geochemical and one for petrographical analysis. Half of each sample was dried, crushed, and pulverised to analytical fineness, and subsequently homogenised. An aliquot of each powder has been shipped to RWTH Aachen (RWTH; Germany) and to SGS Bulgaria LTD laboratory in Serbia for whole-rock geochemical analysis.

Polished sections have been prepared of the other half of the samples. Sections have been shipped to RWTH and were examined under a Leica DM 4500p polarization microscope under reflected light for mineralogic and textural properties at the Institute of Applied Mineralogy and Economic Geology at RWTH.

4.2 pXRF analysis

Sample cups were conventionally prepared at RWTH for pXRF analysis. All cups were covered with a 4.0 µm thick polypropylene film for comparability of results. Portable XRF analysis was performed at Clausthal University of Technology (Germany) using a Niton™ XL3t RFA analyser equipped with a silver anode (6 to 50 kV, 0 to max 200 µA). Both major and trace elements were analysed using the factory standard calibration mining mode with beam count time set to 100 s. For precision and accuracy of the instrument, different OREAS CRMs (OREAS 623, 134b, 932) with varying Zn and Cu contents, reasonably covering the concentration range of the sample suite, were analysed. CRMs were analysed at the beginning and after every fifth sample measurement. Certified values of the used CRMs were compared to the obtained pXRF values for these materials, whereby standard deviations (SD), relative percentage standard deviations (%RSD), and percentage differences (%diff) were calculated. These values were used then to evaluate the precision and accuracy of the instrument. A full spectrum of major and trace element concentrations determined by pXRF is provided in Appendix A.

4.3 ICP-MS/AAA analysis

Conventional ICP-MS/AAS analyses after near total 4-acid digestion were adapted from the same samples. Pulps of all samples were analysed for Ag (0.005), As (1.0), Ce (0.05), Cd (0.01), Co (0.1), Cr (1.0), Cu (0.5), Fe (100), Ga (0.1), In (0.02), La (0.1), Mn (5), Nb (0.1), Pb (2), and Zn (0.5) [lower detection limits, in ppm, are given in brackets] via ICP-MS at the commercial run SGS Bulgaria LTD laboratory in Serbia. Analyses of added internal standards verify ICP-MS results of good quality. Samples with elemental concentrations above the upper detection limit were re-analysed using AAS at the SGS Bulgaria LTD laboratory. All ICP-MS and AAS results of major and trace elements are shown in Appendix B.

5. Results

5.1 Ore mineralogy

The mineralisation is hosted in a medium to coarse-grained dolomitic unit and is largely defined by the ore paragenesis of bornite, chalcopyrite, galena, covellite and chalcocite, mainly associated with quartz and calcite (Fig. 4). Mineralisation is largely structurally-controlled, but quite variable, leading to an overlap of zones of massive, disseminated, and veinlet-controlled ore mineralization styles as well as brecciated mineralized zones. Petrographic ore textures include the following: skeletal (Fig. 4a), replacement (Fig. 4b, d & f), subhedral to anhedral (Fig. 4c & d) and enveloping rims (Fig. 4e). Anhedral, brown coloured bornite is the dominant ore mineral. Bornite is overgrown by thin rims of chalcocite that are commonly associated with galena and pyrite and by fine patches of covellite (Fig. 4c, e & f). Frequently, bornite is replaced by coarse-grained chalcopyrite that can become locally massive (Fig. 4f). Pyrite is mostly medium to coarse grained, exhibiting subhedral to anhedral form and is commonly associated with chalcopyrite and galena and occasionally enclosed within anhedral galena grains (Fig. 4b & d). Covellite is minor and probably of supergene origin. It forms at the outer rims of bornite and is mostly within the bornite-chalcopyrite association. Covellite is irregular, fine-grained, showing a patchy occurrence within bornite grains, probably replacing chalcopyrite (Fig. 4f). Chalcocite is mostly associated with bornite and occurs randomly disseminated in the calcite matrix.

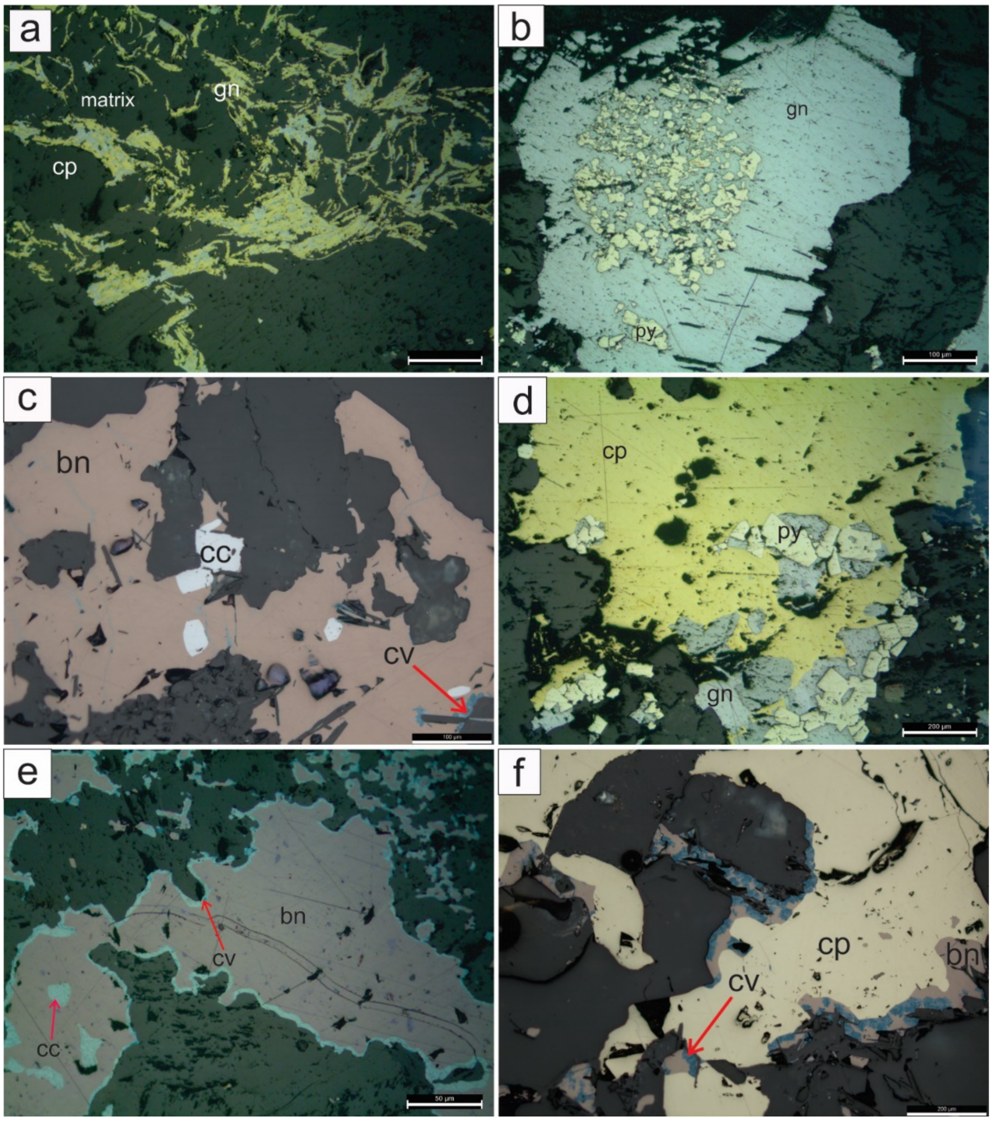

Fig. 4. Photomicrographs in reflected light showing microtextural features of the sulfide ores at Kombat. a) Emulsion texture of massive chalcopyrite and galena embedded in the dolomitic matrix. b) Pyrite grains embedded in galena. c) Coarse bornite grains with rims of covellite and fissures healed with covellite, and minor chalcocite. d) Coarse-grained chalcopyrite with subhedral grains of pyrite embedded within galena grains. e) Replacement of bornite by covellite, with embedded chalcocite. f) Bornite crystals largely replaced by chalcopyrite. Bornite has rims of covellite. Abbreviations: bn-bornite, cc-chalcocite, cp-chalcopyrite, cv-covellite, gn-galena, py-pyrite.

5.2 ICP-MS/AAS vs pXRF

ICP-MS analyses point out quite varying element contents within the sample suite. Non-metal contents such as S and P vary between ≤0.01 and ≤2.5 wt.%. The concentrations of metalloids such as As and Sb vary between ≤0.4 and ≤1,100 ppm, of transitional metals such as Ag, Cd, Cr, Co, Cu, Nb, Mn and Zn vary between ≤0.4 and ≥10,000 ppm, of post-transitional metals such as Pb and Ga vary between ≤0.5 and ≥10,000 ppm and of REEs such as Ce and La vary between ≤1 and ≤2.5 ppm. The concentrations of Ag, Cu, Fe, Pb and Zn analysed by pXRF are all within an acceptable range in comparison to ICP-MS data. There is a high positive linear correlation between pXRF and ICP-MS values for the abovementioned elements as depicted by the R^2 values (coefficient of correlation; R^2 ≥0.90) in Table 1. In contrast, the non-metal elements have a much lower correlation, ranging between 0.6 and 0.8. The analytical concentrations of Cr, Co and Nb were largely below the lower analytical detection limits of the pXRF analyser.

Element correlations were studied in all samples using ICP-MS/AAS obtained data (Table 2). A relatively strong correlation was observed between a number of elements such as: As with Cd and Zn ($R_{As/Cd} = 0.89$; $R_{As/Zn} = 0.98$); Cd and Zn ($R_{Cd/Zn} = 0.86$); Ce with Ga, Tb and Y ($R_{Ce/Ga} = 0.82$; $R_{Ce/Tb} = 0.86$; $R_{Ce/Y} = 0.93$); Cs with K and Rb ($R_{Cs/K} = 0.91$; $R_{Cs/Rb} = 0.91$); Fe with Sr, U and W ($R_{Fe/Sr} = 0.96$; $R_{Fe/U} = 0.89$; $R_{Fe/W} = 0.99$); Ga with Tb, Y and Yb ($R_{Ga/Tb} = 0.88$; $R_{Ga/Y} = 0.87$; $R_{Ga/Yb} = 0.86$); La with P and Y ($R_{La/P} = 0.82$; $R_{La/Y} = 0.86$); Lu with Sr, Tb, Y and Yb ($R_{Lu/Sr} = 0.81$; $R_{Lu/Tb} = 0.94$; $R_{Lu/Y} = 0.87$; $R_{Lu/Yb} = 0.98$); Sr with U and W ($R_{Sr/U} = 0.91$; $R_{Sr/W} = 0.97$); Tb with Y and Yb ($R_{Tb/Y} = 0.95$; $R_{Tb/Yb} = 0.95$); U and W ($R_{U/W} = 0.91$) and Y and Yb ($R_{Y/Yb} = 0.88$).

Table 1. Correlation coefficients applicable to pXRF data.

	Mean (wt.%)	Error	Error (%)	R^2
Ag	0.003	0.001	33	0.99
Cu	0.60	0.008	1.40	0.97
Fe	4.08	0.042	1.03	0.99
Pb	1.79	0.020	1.80	0.96
Zn	1.44	0.023	1.50	0.96

5.3 Precision and accuracy

Assessment of sample precision and instrument precision was done according to the studies of Le Vaillant et al. (2014), Piercey and Devine (2014), and Simandl et al. (2014a). For determination of sample precision, pXRF and ICP-MS/AAS results of four samples from the OML (KC002: brecciated, sulphide-mineralised zone; KH002: chalcopyrite-rich dolomite;

KEN004: coarse grained dolomite, rich in galena; and KEN002: massive, disseminated chalcopyrite and bornite), were examined. The instrument's precision was determined by analysing matrix-matched CRMs (OREAS 932, 134b, 623), with a range of concentration of elements matching the elemental concentration range of the samples.

The instrument's precision of selected elements is illustrated graphically (Fig. 5) using the %RSD obtained from pXRF results of samples combined with the certified values of the CRMs. The %RSD was calculated using equation 1; the accuracy was derived from %diff which was obtained using equation 2.

$$\%\mathrm{RSD} = \frac{\mathrm{SD}}{\bar{\mathrm{x}}(\mathrm{pXRF})} * 100\% \qquad \text{[equation 1]}$$

$$\%\mathrm{diff} = \frac{\bar{\mathrm{x}}(\mathrm{pXRF}) - \mathrm{x}(\mathrm{CV})}{\mathrm{x}(\mathrm{CV})} * 100\% \qquad \text{[equation 2]}$$

Whereby SD is the standard deviation and $\bar{\mathrm{x}}$(pXRF) is the mean of the respective pXRF value. The percentage difference (%diff) represents the deviation of the by pXRF analysed value of a selected element ($\bar{\mathrm{x}}$(pXRF)) of a CRM from the respective certified value of the CRM (x(CV)). The statistical data of the CRMs, including averages, SD, %SRD and %diff are in Appendix C.

Using the classification criteria adopted from Piercey and Devine (2014), the instrument's precision ranges from excellent to very good for Cu, Zn, and Pb with $0.13 \leq \%\mathrm{RSD} \leq 7.4$ (Fig. 5). Similarly, the sample results reveal that Cu, Zn, and Pb show an excellent to very good precision with the exception of one Pb value which is considered as an outlier (sample KH002; RSD ≥10%; Table 3). Accuracy is deduced from the %diff, noting that this is representative of the systematic error for each given element. Accuracy for all elements with %diff values of <10% are considered as excellent, and a value between 10% and 20% as good. All data within these ranges can be used for interpretation, while %diff values of >20% are considered to be too poor according to Hughes and Barker (2018). Certified reference materials yielded good accuracy for Cu, Zn and Pb (%diff ≤15), however, there is at the same time a large variation in sample accuracy for Cu, Zn and Pb ($6 \leq \%\mathrm{diff} \geq 100$).

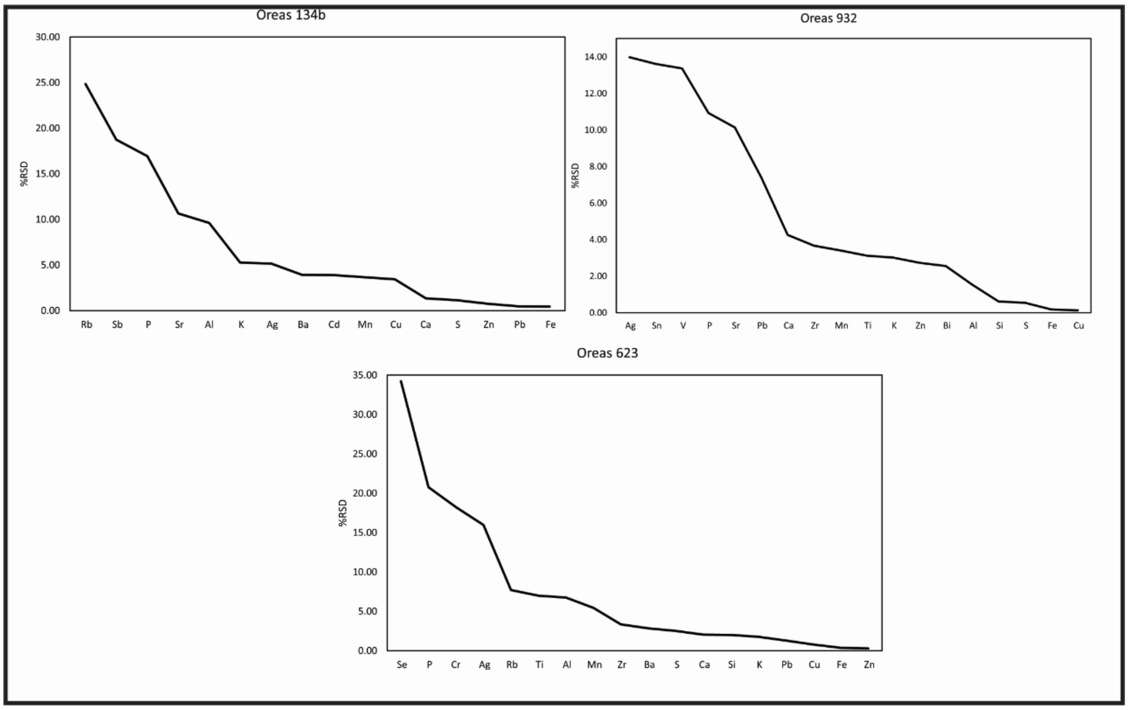

Fig. 5. Line graphs showing the relative standard deviations (%RSD) of pXRF results of certified values of selected elements of the OREAS 37, 134b and 932 CRMs.

Table 2. Correlation coefficient between various elements of the Kombat sulfide mineralization, all analysed by ICP-MS/AAS.

	Ag	As	Cd	Ce	Co	Cr	Cs	Cu	Fe	Ga	K	La	Li	Lu	Mg	Mn	Mo	Ni	P	Pb	Rb	Sb	Sr	Tb	Tl	U	V	W	Y	Yb	Zn
Ag	1																														
As	-0.08	1																													
Cd	0.07	0.89	1																												
Ce	-0.30	-0.04	0.02	1																											
Co	-0.16	0.45	0.50	0.35	1																										
Cr	-0.30	0.21	0.12	0.08	0.06	1																									
Cs	-0.15	0.09	0.13	0.51	0.13	0.11	1																								
Cu	0.76	0.10	0.16	-0.32	-0.05	-0.20	-0.29	1																							
Fe	-0.09	-0.03	0.37	0.16	-0.13	0.02	-0.11	-0.06	1																						
Ga	-0.31	-0.08	0.01	0.82	0.31	-0.09	0.40	-0.42	0.41	1																					
K	-0.22	-0.13	-0.01	0.63	0.15	-0.02	0.91	-0.35	-0.07	0.61	1																				
La	-0.23	-0.25	-0.27	0.81	-0.07	0.17	0.28	-0.34	0.08	0.64	0.41	1																			
Li	-0.23	-0.05	0.02	0.29	-0.02	0.10	0.79	-0.30	-0.20	0.19	0.73	0.10	1																		
Lu	-0.28	-0.11	0.01	0.75	0.12	-0.03	0.27	-0.29	0.71	0.84	0.40	0.60	0.05	1																	
Mg	-0.12	-0.24	-0.26	-0.28	-0.22	-0.19	0.14	-0.28	-0.27	-0.25	0.14	-0.21	0.15	-0.38	1																
Mn	0.19	0.19	0.19	-0.20	-0.13	-0.17	-0.08	0.22	-0.19	-0.29	-0.15	-0.23	0.13	-0.23	-0.18	1															
Mo	-0.17	0.06	0.13	0.56	0.25	0.13	-0.13	-0.14	0.71	0.63	-0.05	0.43	-0.29	0.79	-0.38	-0.18	1														
Ni	-0.09	-0.15	-0.28	0.08	0.02	-0.32	0.15	-0.28	-0.77	-0.02	0.22	0.19	0.20	-0.3	0.14	0.26	-0.51	1													
P	-0.21	-0.27	-0.22	0.74	-0.08	0.00	0.67	-0.40	-0.09	0.61	0.78	0.82	0.49	0.44	0.11	-0.16	0.06	0.33	1												
Pb	-0.09	0.17	0.27	0.13	0.78	0.03	0.09	-0.12	-0.05	0.32	0.20	-0.12	-0.04	0.08	-0.12	-0.34	0.10	-0.04	-0.07	1											
Rb	-0.20	-0.01	0.09	0.59	0.25	0.04	0.91	-0.26	-0.01	0.57	0.97	0.29	0.73	0.37	0.06	-0.08	-0.02	0.08	0.67	0.26	1										
Sb	-0.12	0.64	0.55	-0.04	0.35	0.23	-0.13	0.46	0.07	-0.16	-0.2	-0.23	-0.14	-0.06	-0.31	0.07	0.08	-0.38	-0.31	0.08	-0.04	1									
Sr	-0.11	-0.11	0.03	0.30	-0.16	-0.05	-0.04	-0.19	0.96	0.58	0.05	0.23	-0.15	0.81	-0.28	-0.19	0.75	-0.60	0.06	-0.06	0.07	-0.11	1								
Tb	-0.27	-0.08	0.02	0.86	0.16	0.04	0.36	-0.34	0.54	0.88	0.49	0.75	0.08	0.94	-0.39	-0.3	0.70	-0.18	0.61	0.15	0.44	-0.13	0.67	1							
Tl	-0.15	0.32	0.42	0.62	0.80	0.01	0.34	-0.20	-0.14	0.64	0.47	0.31	0.15	0.32	-0.18	-0.11	0.36	0.18	0.33	0.67	0.50	0.13	-0.04	0.42	1						
U	-0.13	-0.11	0.10	0.26	0.01	-0.03	0.03	-0.22	0.89	0.60	0.14	0.17	-0.15	0.76	-0.25	-0.26	0.64	-0.58	0.08	0.26	0.17	-0.13	0.91	0.67	0.08	1					
V	-0.16	0.20	0.42	0.37	0.60	0.09	0.08	-0.16	0.66	0.56	0.13	0.04	-0.11	0.64	-0.30	-0.18	0.71	-0.55	-0.06	0.59	0.24	0.13	0.63	0.56	0.48	0.77	1				
W	-0.09	-0.10	0.19	0.16	-0.21	0.01	-0.08	-0.15	0.99	0.43	-0.03	0.12	-0.18	0.71	-0.21	-0.19	0.68	-0.70	-0.03	-0.08	0.00	-0.08	0.97	0.57	-0.17	0.91	0.62	1			
Y	-0.32	-0.13	-0.07	0.93	0.18	0.02	0.35	-0.36	0.34	0.87	0.50	0.86	0.12	0.87	-0.35	-0.29	0.66	0.02	0.69	0.07	0.42	-0.13	0.50	0.95	0.48	0.45	0.39	0.36	1		
Yb	-0.31	-0.13	-0.05	0.77	0.13	-0.05	0.29	-0.31	0.69	0.86	0.43	0.60	0.08	0.98	-0.34	-0.3	0.78	-0.32	0.46	0.11	0.41	-0.07	0.79	0.95	0.34	0.76	0.63	0.70	0.88	1	
Zn	-0.09	0.98	0.86	-0.10	0.38	0.21	0.05	0.20	-0.05	-0.15	-0.16	-0.29	-0.05	-0.16	-0.23	0.21	0.00	-0.17	-0.3	0.10	-0.03	0.74	-0.14	-0.14	0.24	-0.15	0.12	-0.13	-0.19	-0.18	1

Table 3. Assessment of sample precision and accuracy of the samples KEN002, KEN004, KC002 and KH002. Abbreviations: SD-standard deviation, %RSD-relative percentage standard deviation, $\bar{x}$(pXRF)-mean pXRF value, CRV-standard certified value, %diff-percentage difference

KEN002					
Element	$\bar{x}$(pXRF)	CRV	SD	%RSD	%diff
Ag	0.001	0.001	0.001	91	186
Ba	0.015	0.001	0.002	14	1775
Cu	0.347	0.544	0.002	0.676	-36
Fe	0.627	0.890	0.006	1.01	-30
Mn	0.565	0.618	0.009	1.53	-8.55
Pb	0.725	1.15	0.004	0.572	-37
Sr	0.016	0.003	0.001	2.83	5.33
S	0.389	2.10	0.010	2.53	-81
Zn	0.007	0.006	0.001	6.21	19
KEN004					
Ag	186	0.001	0.001	0.001	39
Ba	1775	0.029	0.001	0.003	9.12
Cu	-36	2.30	2.15	0.020	0.89
Fe	-30	3.50	3.93	0.006	0.18
Mn	-8.55	0.826	0.784	0.012	1.47
Pb	-37	1.63	1.45	0.009	0.573
Sr	5.33	0.020	0.018	0.005	2.26
S	-81	2.14	4.30	0.053	2.47
Zn	19	0.046	0.038	0.002	3.61
KC002					
Ag	0.001	0.001	0.001	56	31
Ba	0.063	0.051	0.002	2.85	22
Cu	0.652	0.737	0.004	0.546	-11
Fe	0.280	0.260	0.004	1.53	7.54
Mn	0.417	0.458	0.005	1.18	-8.86
Pb	0.066	0.095	0.001	1.74	-31
Sr	0.011	0.011	0.000	0.000	3.77
S	0.072	1.30	0.002	2.09	-94
Zn	0.005	0.002	0.001	24	113
KH002					
Ag	0.001	0.001	0.001	37	97
Ba	0.009	0.002	0.002	19	462
Cu	4.66	6.91	0.028	0.600	-32
Fe	4.89	5.27	0.013	0.271	-7.15
Mn	0.523	0.488	0.006	1.1	7.19
Pb	0.003	0.002	0.001	21	53
Sr	0.014	0.013	0.001	3.15	5.97
S	2.44	3.50	0.052	2.12	-30
Zn	0.046	0.038	0.002	4.73	22

Iron and Mn values are of excellent to very good precision (0.1 ≤ %RSD ≤ 3.6) for both samples and CRMs. There is a slight variation in accuracy for Fe values in both CRMs and samples, ranging from very good to poor. Manganese, in contrary to Fe, yields a better accuracy in both samples and CRMs. Both Ag and Ba have low precision and accuracy in CRMs and samples. Certified reference materials with an average concentration of Ag of 0.02 wt.% have a fairly good precision with ≤5.5%, but a relatively poor accuracy of only ≤25%.

6. Discussion

6.1 Ore mineral assemblage and trace element abundance at Kombat

The Kombat deposit can be described as a discordant, structurally-controlled sulfide mineralization with a complex mineralogy. It is classified as cupriferous Tsumeb-type deposit by Frimmel et al. (1996), Melcher (2003), and Kamona and Günzel (2007). Chalcopyrite, bornite, pyrite and galena are the most abundant sulfide minerals, with minor occurrences of covellite and chalcocite (Fig. 4). Chalcopyrite, bornite, pyrite and galena are mainly fine to medium grained and subhedral. The minor minerals either occur as intergrowths or rims surrounding the primary ore minerals (Fig. 4).

Out of all 49 elements analysed, at least 12 trace elements are present in measurable concentrations and have an arithmetic mean that is above bulk continental crust (bcc) estimates (Fig. 6; data for comparison from Rudnick and Gao, 2003). There is a clear enrichment of Pb, Cu, Ag, As, Cd, S and Sb, and a less pronounced enrichment of Mn, Mo and P compared to bcc. Most major elements show a slight depletion compared to bcc or are neither enriched nor depleted. Lithophile elements such as Rb, Hf and U are significantly depleted (with mean values ranging between 0.02 and 0.70 ppm) compared to bcc, with exception of W and Mn (mean 1.71-9.41 ppm) which are moderately enriched. Siderophile elements such as Fe, Co and Ni are largely depleted (mean 0.10-0.55 ppm); however, P shows a somewhat enrichment with a mean of 7 ppm. Most of the chalcophile elements are enriched in comparison to bcc. The highest enrichment is observed in Pb, Cu, As and Ag (mean 115-680 ppm), which are at least 100 times more than the average bcc, but Bi and Ga are depleted (mean <0.3 ppm). These elements are all associated with the bornite-chalcopyrite-galena mineral assemblage. Bowell (2014) and Bowell and Mocke (2019) described a variety of As-bearing minerals that are typical for the Tsumeb deposit and since the Kombat deposit is classified as a ‘Tsumeb-type deposit’, it is likely that the enrichment of As in the Kombat deposit as shown in Fig. 6, can be correlated to the presence of As-bearing minerals.

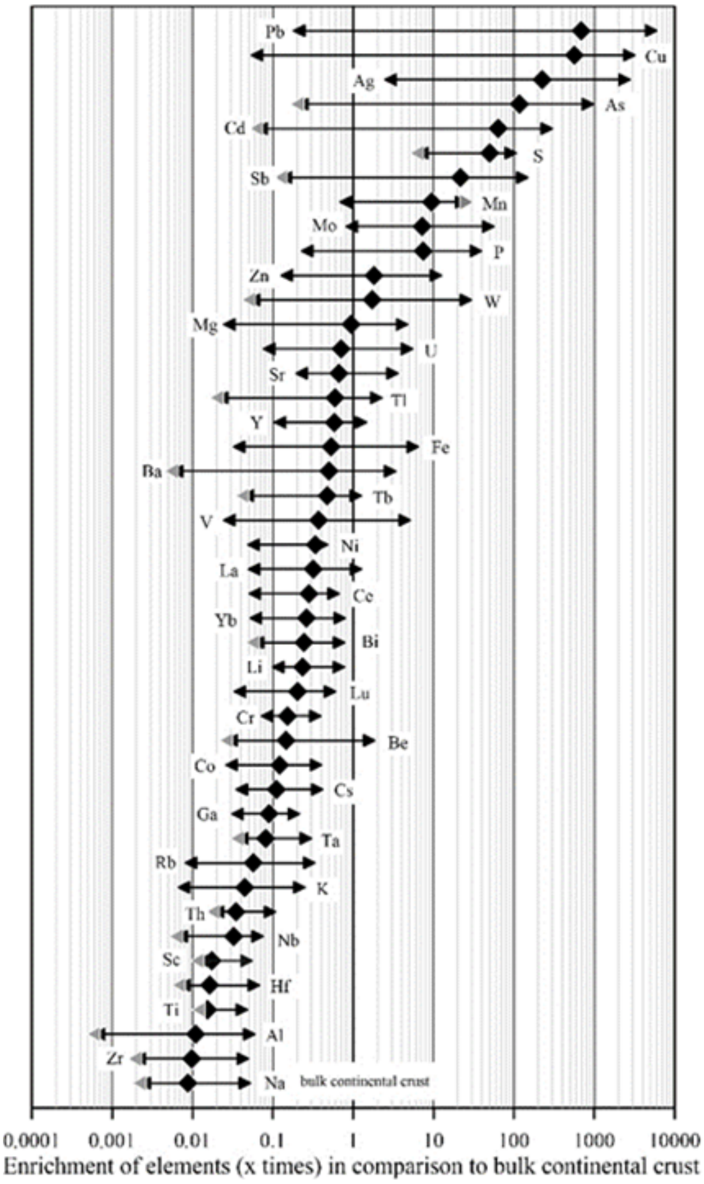

Fig. 6. Enrichment of elements of Kombat ore in comparison to bulk continental crust (data from Rudnick and Gao, 2003) based on ICP-MS data. Squares reflect the arithmetic mean; arrows reflect the concentration range of each element. If elements have values below analytical detection limit (grey arrow tip) the lower element range was set to half lower detection limit. All values below analytical detection limit are considered with half detection limit.

6.2 pXRF as a geochemical exploration method in OML

The evaluation of the correlation or match of pXRF results and ICP-MS results is done using the coefficient of determination (R^2; Fig. 7). There is a strong correlation between values of samples obtained via pXRF and laboratory-driven ICP-MS/AAS values for most of the metallic elements of interest, e.g., Ag ($R^2 = 0.99$), Cu ($R^2 = 0.97$), Fe ($R^2 = 0.99$), Pb ($R^2 = 0.96$) and Zn ($R^2 = 0.96$). Most elements including Cu, Pb and Zn were measured with an adequate accuracy by pXRF (%diff ≤10), based on the precision qualification from Piercey and Devine (2014). However, this is mostly only applicable when element concentrations are well above the lower detection limit of the instrument. If elements are low to very low in concentration, there seems to be an underestimation of values by pXRF. Additionally, elements with a low concentration, such as Ag, have the highest analytical error (Table 1).

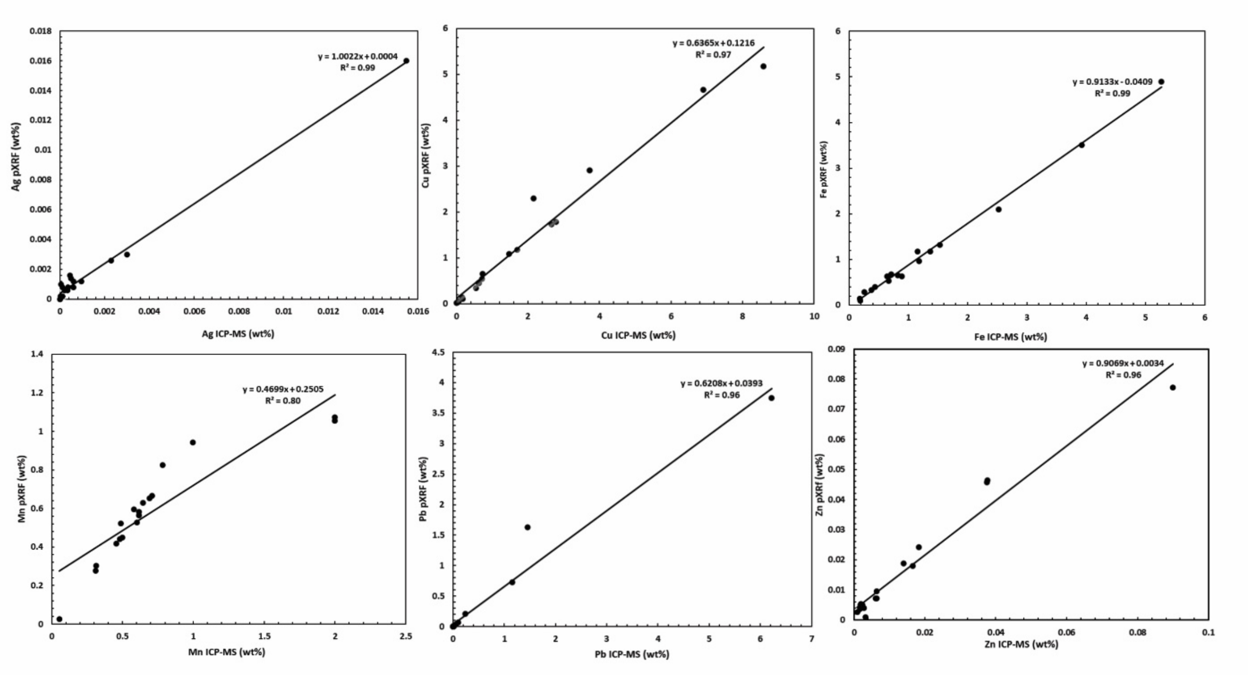

Fig. 7. Regression plots of the elements Ag, Cu, Fe, Mn, Pb and Zn analysed by both ICP-MS (data on x-axis) and XRF (data on y-axis) to show the linear relation, expressed by the coefficient of correlation (R^2), between both methods.

Most of the trace elements detected by ICP-MS such as Ga (0.5–3.4 ppm/0.1 ppm), Nb (<0.1–0.6/0.1 ppm), Cr (9.8–53/1.0 ppm), V (3.4–82.5/1.0 ppm) and W (0.2–29.4/0.1 ppm) were not picked up by the pXRF (first numbers in brackets reflect the concentration range of the element in the samples obtained by ICP-MS; the third number is the lower analytical detection limit by the used ICP-MS device at SGS). This is mostly because they are too low in concentration and well below the detection limit of pXRF, and because of the factory calibration of the device. The lower analytical detection limits of the ICP-MS for these elements are in the range of 0.1–1 ppm, while they are in the range of >>10 ppm for the pXRF method. Therefore, these trace elements could not be detected by the instrument. In cases when the elements cannot be detected by the instrument, either due to low concentration or factory calibration of the instrument, pathfinder elements might be used to infer the presence of those trace elements. Pathfinder elements are elements that have a specific correlation with the selected trace element(s) and can be analyzed by the pXRF accurately and precisely instead of the target element(s) (Hall et al., 2016; Balaram and Sawant, 2022).

Regression analysis of ICP-MS values reveals no positive linear correlation between any element detectable by ICP-MS plus pXRF and any element detectable by ICP-MS but not by pXRF. The only observed positive linear correlations in the ICP-MS dataset are between Y and Yb, Y and Tb, Y and Lu, Yb, and Lu (Fig. 8). However, these five elements cannot be measured using pXRF, and therefore they cannot be used as pathfinders for this purpose. For that reason, it can be argued that pXRF is an effective rapid tool in geochemical exploration for the analysis of selected elements like Ag, Cu, Fe, Pb and Zn in carbonate-hosted sulfide mineralized zones. However, there is still a need to pair pXRF with other traditional geochemical analytical methods to get an overview of the whole elemental concentration spectrum as certain elements cannot be analysed directly by pXRF.

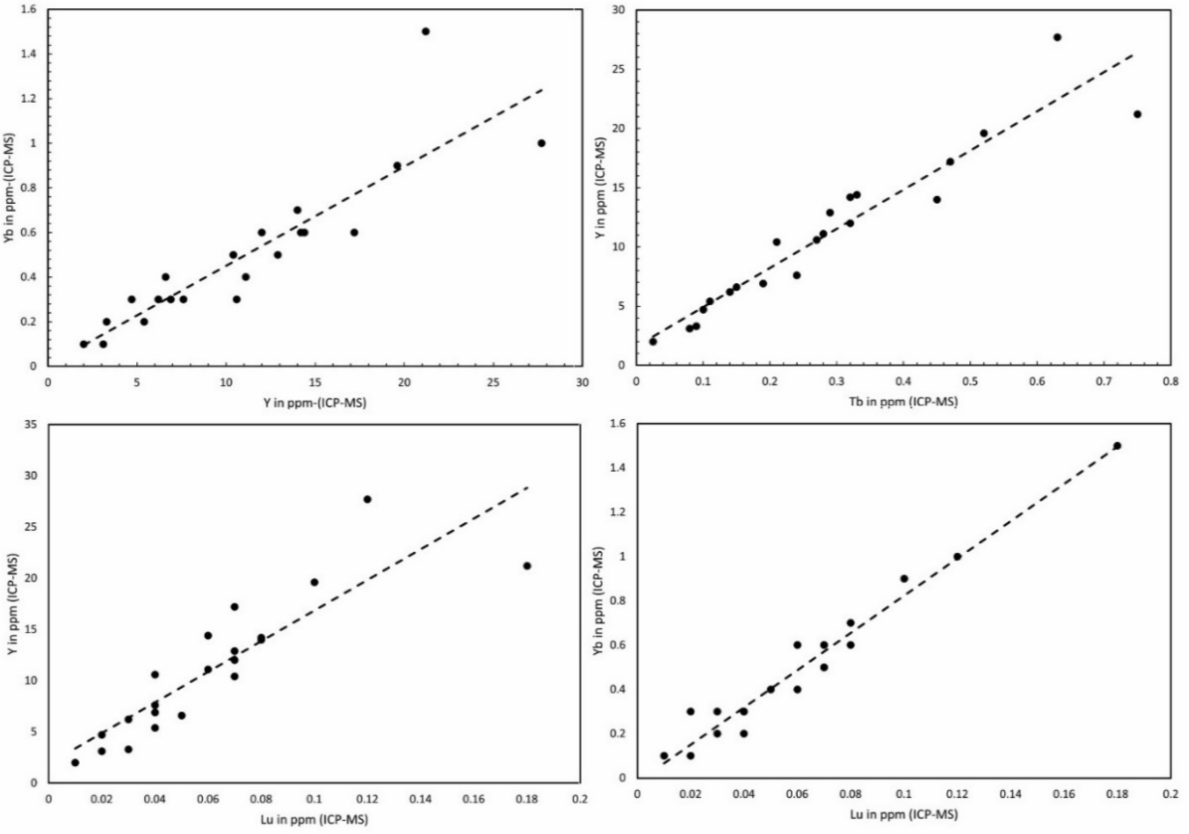

Fig. 1 Binary plots showing positive correlations between selected elements analysed by ICP-MS. a) Y vs. Y. b) Tb vs. Y. c) Lu vs. Y. d) Lu vs. Yb.

7. Conclusion

Portable XRF results for carbonate-hosted Pb-Zn-Ag ores match adequately well with those obtained using ICP-MS for the same samples. This indicates that pXRF is capable to detect the concentration of selected trace elements, with sufficient precision and accuracy, in carbonate-hosted sulphide mineralized zones; and can thus be used as a successful geochemical exploration tool for these types of sulphide ore deposits. However, when the metal concentration is relatively low, there is a quantitative under-estimation of trace element values by pXRF. Nevertheless, pXRF is an effective low-cost method that can be easily used in geochemical exploration to obtain quantitative results of selected metal concentrations of sulfide mineralized zones. Since Kombat sulfide ore contains not only Cu but also other valuable elements, such as Pb, Ag and As, exploring similar carbonate-hosted deposits with pXRF tools could be a suitable approach for projects with limited access to costly laboratory facilities. However, pXRF is not capable of analysing for Ga, Ge and other trace elements when present in low concentrations for which the Otavi Mountain Land deposits are well-known.

8. Acknowledgement

This research is part of a PhD study which is funded by the German Federal Ministry of Education and Research (BMBF) providing financial support through the LoCoSu project (grant number 01DG16011). Many thanks to the staff of the Mineral Resources Department of Clausthal University of Technology for providing access to their pXRF instrument and to Trigon Metal for granting us permission to collect samples on site.

9. References

Andrew, B.S., Barker, S.L., 2017. Determination of carbonate vein chemistry using portable X-ray fluorescence and its application to mineral exploration. Geochemistry: Exploration, Environment, Analysis, 18, 85-93. https://doi.org/10.1144/geochem2016-011.

Arne, D.C., Jeffress, G.M., 2014. Sampling and analysis for public reporting of portable X-ray fluorescence data under the 2012 edition of the JORC code. Proceedings of the Sampling 2014 Conference, Perth.

Balaram, V., Sawant, S.S. 2022. Indicator minerals, pathfinder elements, and portable analytical instruments in mineral exploration studies. Minerals, 12, 394. https://doi.org/10.3390/min12040394

Boni, M., Terracciano, R., Evans, N.J., Laukamp, C., Schneider, J., Bechstädt, T., 2007. Genesis of vanadium ores in the Otavi Mountainland, Namibia. Economic Geology, 102, 441-469. https://doi:10.2113/gsecongeo.102.3.441.

Bowell, R.J., 2014. Hydrogeochemistry of the Tsumeb deposit: Implications for arsenate mineral stability. Mineralogy and Geochemistry, 79, 589-627. https://doi.org/10.2138/rmg.2014.79.14.

Bowell, R.J., Mocke, H., 2019. Minerals new to Tsumeb. Communications of the Geological Survey of Namibia, 19, 20-46.

Brand, N.W., Brand C.J., 2014. Performance comparison of portable XRF instruments. Geochemistry: Exploration, Environment, Analysis, 14, 125-138. http://dx.doi.org/10.1144/geochem2012-172.

Cairncross, B., 1997. The Otavi Mountain Land Cu-Pb-Zn-V Deposits, Namibia. Mineralogical Record, 28, 109-130.

Cairncross, B., 2021. Minerals of Berg Aukas, Otavi Mountainland, Namibia. Rocks and Minerals, 96, 110-147. https://doi.org/10.1080/00357529.2021.1848216

Chetty, D., Frimmel, H.E., 2000. The role of evaporites in the genesis of base metal sulphide mineralisation in the Northern platform of the PanAfrican Damara belt, Namibia. Geochemical and fluid inclusion evidence from carbonate wall rock alteration. Mineralium Deposita, 35, 364-375. https://doi.org/10.1007/s001260050247.

Deane, J.G., 1995. The structural evolution of the Kombat deposit, Otavi Mountain Land, Namibia. Communications of the Geological Survey of Namibia, 10, 99-107.

Fisher, L., Gazley, M.F., Baensch, A., Barnes, S.J., Cleverley, J., Duclaux, G., 2014. Resolution of geochemical and lithostratigraphic complexity: a workflow for application of portable X-ray fluorescence to mineral exploration. Geochemistry: Exploration, Environment, Analysis, 14, 149-159. https://doi.org/10.1144/geochem2012-158.

Frimmel, H.E., Deane, J.G., Chadwick, P.J., 1996. Pan-African tectonism and the genesis of base metal sulfide deposits in the northern foreland of the Damara Orogen, Namibia. Society of Economic Geologists Special Publication, 4, 204-217.

Gallhofer, D., Lottermoser, B.G., 2018. The influence of spectral interferences on critical element determination with portable X-ray fluorescence (pXRF). Minerals, 8, 320. https://doi:10.3390/min8080320

Gazley, M.F., Fisher, L.A., 2014. A review of the reliability and validity of portable X-ray fluorescence spectrometry (pXRF) data. In: Gazley, M.F., Fisher, L. (eds) Mineral resource and ore reserve estimation – the AusIMM guide to good practice. The Australasian Institute of Mining and Metallurgy. Melbourne 69-82.

Goscombe, B., Gray, D., Hand, M., 2004. Variation in metamorphic style along the northern margin of the Damara Orogen, Namibia. Journal of Petrology, 45, 1261-1295. https://doi.org/10.1093/petrology/egh013.

Goscombe, B., Foster, D.A., Gray, D., Wade, B., 2018. The Evolution of the Damara Orogenic System: A record of West Gondwana assembly and crustal response. In: Siegesmund, S., Oyhantçabal, P., Basei, M.A.S., Oriolo, S. (eds) Geology of Southwest Gondwana. Regional Geology Reviews. https://doi.org/10.1007/978-3-319-68920-3_12.

Gray, D., Foster, D., Meert, J., Goscombe, B., Armstrong, R., Trouw, R., Passchier, C., 2008. A Damara orogen perspective on the assembly of southwestern Gondwana. Geological Society Special Publication, 294, 257-278. https://doi.org/10.1144/SP294.14.

Haest, M., Muchez, P., 2011. Stratiform and vein-type deposits in the pan-African orogen in Central and Southern Africa: Evidence for multiphase mineralisation. Geologica Belgica, 14, 23-44.

Hall, G.E., Bonham-Carter, G.F., Buchar, A., 2014. Evaluation of portable X-ray fluorescence (pXRF) in exploration and mining: Phase 1, control reference materials. Geochemistry: Exploration, Environment, Analysis, 14, 99-123. https://doi.org/10.1144/geochem2013-241.

Hall, G.E.M., McClenaghan, M.B., Pagé, L., 2016. Application of portable XRF to the direct analysis of till samples from various deposit types in Canada. Geochemistry: Exploration, Environment, Analysis, 16, 62-84. https://doi.org/10.1144/geochem2015-371

Hoffman, P.F., 2011. Strange bedfellows: glacial diamictite and cap carbonate from the Marinoan (635 Ma) glaciation in Namibia. Sedimentology, 58, 57-119. https://doi.org/10.1111/j.1365-3091.2010.01206.x

Hoffman, P.F., 2013. The tooth of time: Henno Martin. Geoscience Canada, 40, 17-31.

Hughes, R., Barker, S.L., 2018. Using portable XRF to infer adularia halos within the Waihi Au-Ag system, New Zealand. Geochemistry: Exploration, Environmental, Analysis, 18, 97-108. https://doi.org/10.1144/geochem2016-006.

Kamona, F., Günzel, A., 2007. Stratigraphy and base metal mineralization in the Otavi Mountain Land, northern Namibia- a review and regional interpretation. Gondwana Research, 11, 396-413. https://doi.org/10.1016/j.gr.2006.04.014.

Kröner, A., 1982. Rb–Sr geochronology and tectonic evolution of the Pan-African Damara belt of Namibia, southwestern Namibia. American Journal of Science, 282, 1471-1507. https://doi.org/10.2475/ajs.282.9.1471

Leach, D.L., Bradley, D.C., Huston, D., Sergei, P.A., Ryan, T.D., Steven, G.J., 2010. Sediment-hosted lead-zinc deposits in earth history. Economic Geology, 105, 593-625. https://doi.org/10.2113/gsecongeo.105.3.593

Lemière, B., 2018. A review of pXRF (field portable X-ray fluorescence) applications for applied geochemistry. Journal Geochemical Exploration, 188, 350-363. https://doi.org/10.1016/j.gexplo.2018.02.006.

Le Vaillant, M., Barnes, S.J., Fisher, L., Fiorentini, M.L., Caruso, S., 2014. Use and calibration of portable X-ray fluorescence analysers: Application to lithogeochemical exploration for komatiite-hosted nickel sulphide deposits. Geochemistry: Exploration, Environment, Analysis 14, 199-209. https://doi.org/10.1144/geochem2012-166.

Martin, H., Porada, H., 1977. The intracratonic branch of the Damara orogen in southwest Africa I. Discussion of geodynamic models. Precambrian Research, 5, 311-338. https://doi.org/10.1016/0301-9268(77)90039-0.

Melcher, F., 2003. The Otavi Mountainland in Namibia: Tsumeb, germanium and snowball Earth. Mitteilungen der Österreichischen Mineralogischen Gesellschaft, 148, 413-435.

Melcher, F., Oberthür, T., Rammlmair, D., 2006. Geochemical and mineralogical distribution of germanium in the Khusib Springs Cu-Zn-Pb-Ag sulphide deposit, Otavi Mountain Land, Namibia. Ore Geology Reviews, 28, 32-56. https://doi.org/10.1016/j.oregeorev.2005.04.006

Miller, R.M., 1983. The Pan-African Damara Orogen of South West Africa/Namibia. In: R. McG. Miller (ed) Evolution of the Damara Orogen of South West Africa/Namibia. Special Publication of the Geological Society of South Africa, 11, 431-515.

Miller, R.M., 2008. Neoproterozoic and early Palaeozoic rocks of the Damara Orogen. In: Miller, R.M. (ed), The Geology of Namibia, 2. Geological Survey of Namibia, Windhoek, 13-1–13-410

Minz, F., 2008. The Kombat ore deposit, Otavi Mountain Land (Northern Namibia). Research project, Freiber University of Mining and Technology.

Nghoongoloka, A., Bowell, R., Kamona, A.F., Mocke, H., 2020. Re-evaluation of Kombat-style mineralization and implications for exploration in the Otavi Mountain Land, Namibia. Open Journal of Geology, 10, 1119-1152. https://doi.org/10.4236/ojg.2020.1011054.

Piercey, S.J., Devine, M.C., 2014. Analysis of powdered reference materials and known samples with a benchtop, field portable X-ray fluorescence (pXRF) spectrometer: Evaluation of performance and potential applications for exploration lithogeochemistry.

Geochemistry: Exploration, Environment, Analysis, 14, 139-148, https://doi.org/10.1144/geochem2013-199.

Pirajno, E., Joubert, B.D., 1993. An overview of carbonate-hosted mineral deposits in the Otavi Mountain Land, Namibia: Implications for ore genesis. Journal of African Earth Sciences, 6, 265-272. https://doi.org/10.1016/0899-5362(93)90048-U.

Porada, H., 1979. The Damara-Ribeira orogen of the Pan-African/Brasiliano cycle in Namibia (Southwest Africa) and Brazil as interpreted in terms of continental collision. Tectonophysics, 57, 237-265. https://doi.org/10.1016/0040-1951(79)90150-1

Quye-Sawyer, J., Vandeginste, V., Johnston, K.J., 2015. Application of handheld energy-dispersive X-ray fluorescence spectrometry to carbonate studies: Opportunities and challenges. Journal of Analytical Atomic Spectrometry, 30, 1490-1499. https://doi.org/10.1039/C5JA00114E

Rudnick, R.L., Gao, S., 2003. The composition of the continental crust. Treatise on Geochemistry, 3, 1-64. http://dx.doi.org/10.1016/b0-08-043751-6/03016-4.

Schneider, J., Boni, M., Laukamp, C., Bechstädt, T., Petzel, V., 2008. Willemite (Zn_2SiO_4) as a possible Rb–Sr geochronometer for dating nonsulfide Zn–Pb mineralization: Examples from the Otavi Mountainland (Namibia). Ore Geology Reviews, 33, 152–167. https://doi.org/10.1016/j.oregeorev.2006.05.012

Simandl, G.J., Fajber, R., Paradis, S., 2014a. Portable X-ray fluorescence in the assessment of rare earth element enriched sedimentary phosphate deposits. Geochemistry: Exploration, Environment, Analysis, 14, 161-169. https://doi.org/10.1144/geochem2012-180.

Simandl, G.J. Stone, R.S., Paradis, S., Fajber, R., 2014b. An assessment of a handheld X-ray fluorescence instrument for use in exploration and development with an emphasis on REEs and related specialty metals. Mineralium Deposita, 49, 999-1012. https://doi.org/10.1007/s00126-013-0493-0.

Trigon Metals Inc, 2017. NI 43-101 Technical report on the Kombat copper project, Namibia Mineral Resource Report.

Xiong, S.F., Jiang, S.Y., Ma, Y., Liu, T., Zhao, K.D., Jiang, M.R., Zhao, H.D., 2019. Ore genesis of Kongxigou and Nanmushu Zn-Pb deposits hosted in Neoproterozoic carbonates, Yangtze Block, SW China: Constraints from sulfide chemistry, fluid inclusions, and in situ S-Pb isotope analyses. Precambrian Research, 333, 105405. https://doi.org/10.1016/j.precamres.2019.105405

Young, K.E., Evans, C.A., Hodges, K.V., Bleacher, J.E., 2016. A review of the handheld X-ray fluorescence spectrometer as a tool for field geologic investigations on Earth and in planetary surface exploration. Applied Geochemistry, 72, 77-87. https://doi.org/10.1016/j.apgeochem.2016.07.003